Chapter 3
Near-Time Sea Surface Temperature and Tropical Cyclone Intensity in the Eastern North Pacific Basin

Jerry Y. Jien, William A. Gough, Ken Butler, Vincent Cheng, and George Arhonditsis

Abstract Although a significant relationship between near-time sea surface temperature (SST) and tropical cyclone (TC) intensity has been found for many major TC basins, this topic has not been explored in the eastern North Pacific (ENP) basin. When the main development region of the (ENP) Ocean is subdivided into eastern (EDR) and western (WDR) development regions, SSTs show a weak, yet significant, positive relationship with intensities of the six-hourly TC observations and storms' maximum strengths only in the WDR. This SST-storm intensity relationship is most apparent for the maximum lifetime TC intensity of WDR major hurricanes. The maximum strength of major hurricanes in the ENP basin is more clearly established in the WDR where SST is at least 25 °C, well below the minimum SST value that is observed in the North Atlantic basin.

When intensity observations are binned into SST intervals, the upper bound value of TC intensity is found to increase with SST. Compared to the previous TC climatological analysis (Whitney and Hobgood (1997) J Clim 10(11):2921–2930), the maximum relative wind speed has increased for SST bins of 27 °C (>26.5 °C and <27.5 °C) or higher. While a linear function was determined previously as the best empirical fit for the ENP maximum potential intensity (ENPMPI) for each SST bin (Whitney and Hobgood (1997) J Clim 10(11):2921–2930), other means of curve fitting such as the exponential decay (increase form) function also show skill at representing the SST-dependent ENPMPI in the WDR. When storm observations are regionally stratified, the rate of increasing maximum potential intensity with SST flattens out towards the highest SST category. Under the ambient condition in which

J.Y. Jien (✉) • W.A. Gough • V. Cheng • G. Arhonditsis
Department of Physical and Environmental Sciences, University of Toronto Scarborough, 1265 Military Trail, Scarborough, Ontario M1C 1A4, Canada
e-mail: jerry.jien@mail.utoronto.ca; gough@utsc.utoronto.ca; vi.cheng@utoronto.ca; georgea@utsc.utoronto.ca

K. Butler
Department of Computer and Mathematical Sciences, University of Toronto Scarborough, 1265 Military Trail, Scarborough, Ontario M1C 1A4, Canada
e-mail: butler@utsc.utoronto.ca

the theoretical MPI is assumed along ENP storm tracks, the updated relationship of the outflow temperature with SST resembles an inverse (negative) sigmoid curve.

Keywords Sea surface temperature • Eastern North Pacific basin • Tropical cyclone intensity • Maximum potential intensity • Western development region • Eastern development region • Exponential decay • Outflow temperature • Maximum lifetime intensity • Correlation • Statistical relationship • Empirical function • Relative wind speed • Sea surface temperature bin

1   Introduction

Sea surface temperatures (SSTs) have been long thought to be one of the major determining factors in limiting the structure and development of tropical cyclones (Miller 1958; Gray 1968; Merrill 1988; Evans 1993; DeMaria and Kaplan 1994; Whitney and Hobgood 1997; Saunders and Lea 2008). Spatial differences of SST anomalies have also been associated with the interannual variability of the El Niño–Southern Oscillation (ENSO) signal to influence regional tropical cyclone (TC) activity (Chu 2004; Diamond et al. 2013; Wood and Ritchie 2013; Patricola et al. 2014; Zhang and Wang 2015; Boucharel et al. 2016) and landfall impacts (Landsea et al. 1998; Goldenberg et al. 2001; Raga et al. 2013; Martinez-Sanchez and Cavazos 2014) due to changes in TC strength. However, recent research indicates that the development of TCs depends on more than just the absolute value of SST. As confirmed in the data-sparse eastern North Atlantic basin (Wu et al. 2010), Vecchi and Soden (2007), for example, noted that local differences in SST from the zonal or all-tropical mean provided a more effective metric to account for TC intensification than local SST itself. Such derivation of "relative SST" has shown a significant relationship to the storm intensity index (Zhang and Wang 2015) and some practicality in the field of seasonal TC forecast (Caron et al. 2015) in the eastern North Pacific (ENP) basin, where TCs are most active on a per unit area and time (Collins and Roache 2011). Despite this remote/regional control of the local TC intensity, the near-time SST remains one of the primary indicators in regulating the upper boundary of storm intensity and its lifetime maximum wind speed.

Miller (1958) proposed a direct relationship between SST and the minimum sea-level pressure in the surrounding air below the storm eye. Within the context of future climate change scenarios, Emanuel (1987) pointed out that the maximum reduction in sea-level pressure experienced through SST warming pertains only to the reduction of the lowest sustainable pressure achieved by the most intense TC. While a range of environmental conditions could influence the lifetime storm intensity (Gray 1968), SST has been acknowledged to influence a storm's maximum lifetime intensity. However, this direct relationship appears to be less important at explaining TC intensity above a certain SST value (Evans 1993; Michaels et al. 2006). For example, because dynamic forcings such as vertical wind shear are found to be key in determining the intensities of North Atlantic storms (Gray 1984;

Saunders and Lea 2008), it appears TC intensity could be more sensitive to other factors such as atmospheric dynamical influences rather than a single thermodynamic limit alone (Michaels et al. 2006).

SSTs have been found to act as a cap to limit TC intensity at a global scale (Merrill 1988), while outflow temperature at the upper troposphere is critical at determining its maximum potential intensity (MPI; Bister and Emanuel 1998). Using the most reliable storm observations for each TC development basin, intensity data were binned according to the corresponding SST groups to derive empirical relationships of SSTs and their maximum sustained TC winds for the North Atlantic Ocean (DeMaria and Kaplan 1994), Northwestern Pacific Ocean (Zeng et al. 2007) and ENP Ocean (Whitney and Hobgood 1997) and, most recently, Bay of Bengal (Kotal et al. 2009), part of the North Indian basin. While the extent of the relationship of SST-TC intensity varies among basins, a positive correlation between the maximum TC intensity and SST is generally agreed for all TC areas. However, the fact that most TCs do not achieve their SST-bounded MPI suggests other mechanisms are at play.

Instead of assigning each TC observation according to the SST group that it was detected, maximum sustained winds of all TC tracks were directly linked to SST values (Evans 1993; Michaels et al. 2006). However, results of correlating SST values with TC intensities of multiple basins also caution against the overreliance of a single SST predictor at explaining the sustained maximum TC winds (Evans 1993; Henderson-Sellers et al. 1998; Goldenberg et al. 2001). Such an attempt to determine the nature of the SST-TC relationship is further complicated by a storm's self-inflicted SST cooling along its tracks (Mei and Pasquero 2013). Using a relatively higher-resolution SST dataset, Michaels et al. (2006) shared a similar concern in addressing TC intensification by using SSTs alone. Although an SST threshold of 28.25 °C had been determined for North Atlantic TCs to reach major hurricane strength (50 m s^{-1} or greater), further SST warming does not substantially contribute to the rise of maximum TC wind speeds (Michaels et al. 2006).

Observations of TC intensity have been linked to climatological SSTs in multiple basins (Evans 1993) and updated for the North Atlantic TCs (Michaels et al. 2006). However, such research for the ENP basin has been only presented in Whitney and Hobgood (1997) but has not yet been evaluated statistically. Though it had been determined that ENP storm intensities respond to SST change as found in other basins (Evans 1993; Michaels et al. 2006), there may be differences in which ENP storm intensity shows its SST dependence. For instance, ENP storm intensity may be more responsive to thermodynamic limitation when ocean heat sources from both the sea surface and thermocline are considered (Balaguru et al. 2013; Jin et al. 2014). In addition, spatial pattern of SST anomalies may be expressed through ENSO in contrasting storm strength and impacts between local hurricane seasons (Raga et al. 2013; Wood and Ritchie 2013; Martinez-Sanchez and Cavazos 2014). Nevertheless, a direct attribution of near-time SST values to TC winds would also be an improvement over previous basin-wide studies (Emanuel 2005; Webster et al. 2005) and reveal how contemporaneous SST would facilitate the ultimate TC intensity at different levels of storm strength.

The effect of SST on maximum ENP storm intensity was better understood by attributing the SST category as a determining factor on the upper bound of MPI. Based on the exponential function in fitting the maximum TC intensity using SST in the North Atlantic basin (DeMaria and Kaplan 1994), a linear function has been extended for ENP storms (Whitney and Hobgood 1997). After all storms' translational speeds have been removed from the six-hourly observations of sustained winds, the eastern Pacific MPI (EPMPI; m s^{-1}) is developed as such:

$$\text{EPMPI} = C_0 + C_1 \, (\text{SST}), \tag{3.1}$$

whereas SST ($^\circ$C) is associated with a slope (parameter estimate) of $C_1 = 79.17262$ m s^{-1} and a y-intercept (constant) of $C_0 = 5.361814$ m s^{-1} $^\circ$C^{-1}. However, it has been nearly two decades since this empirical relationship on the effect of SST on maximum ENP storm intensity was first documented (Whitney and Hobgood 1997). Due to the SST warming observed worldwide (Xie et al. 2010) and locally (Ralph and Gough 2009), we hypothesize that the upper bound of maximum ENP storm intensity should have also shifted. If this direct relationship holds, then EPMPI pertaining to each SST group is expected to increase as well. As such, the SST-dependent theory of MPI can be refined using the most recent (1982–2013) SST climatological dataset which has a higher temporal-spatial resolution.

The objective of this study is to quantify and update the relationship between TC intensity and its underlying SSTs for ENP storms. Though there is more than one convention (Collins and Mason 2000; Ralph and Gough 2009) to derive the longitudinal boundary as to how the main development region of the ENP basin should be subdivided, to better understand its relationship with its environment, there is a general agreement that the local storm activity should be longitudinally stratified into eastern (EDR; 10–20°N and 85–112°W) and western (WDR; 10–20°N and 112–140°W) development regions. Hence, regional differences of how TC intensity responds to SST fluctuation will be investigated. Given the previous understanding of the regional sensitivity to environmental influences (Collins and Mason 2000; Ralph and Gough 2009; Jien et al. 2015), it is expected that intensities of all WDR storm observations and their lifetime maxima would be more sensitive to SST changes.

Section 2 describes details of the TC and SST datasets and methods used to analyze them. Section 3 provides one rationale for dividing the ENP basin longitudinally when examining possible environmental linkages. In Sect. 4 we explore the spatial misalignment of the warmest SST and maximum storm intensity. Section 5 explores the impact of SST on the maximum lifetime intensity. Section 6 updates the empirical functions by incorporating SST as the dependent variable using the most recent TC climatology. As an update from the work of Whitney and Hobgood (1997), Sect. 7 relates to the update of the outflow temperature at the top of storm clouds (assuming ambient MPI is attained), followed by conclusion in Sect. 8.

2 Data and Methods

Storm track data from the Central Pacific region and eastern North Pacific basins are retrieved from the best track HURDAT2 (Landsea and Franklin 2013) of the National Hurricane Center. This dataset records TC characteristics such as a storm's 1-min maximum sustained wind speed and its geographic positions at six-hourly intervals. Although non-developing tropical depressions are better integrated in the current storm dataset, the possible incompleteness of the early record led to our exclusion of storm data during the pre-satellite era. Due to uncertainty in wind speed estimation below the tropical storm designation, all non-developing tropical depressions are excluded in our analysis.

Modifications from the previous HURDAT (Davis et al. 1984) version include the maximum radii distances of 34 kt (18 m s^{-1}), 50 kt (26 m s^{-1}) and 60 kt (31 m s^{-1}) at all four quadrants of cardinal directions. In addition, reports of storm track positions other than the synoptic (00, 06, 12 and 18 Z) timeframes, when locations of intensity maxima and landfalls are detected, were recently added to the storm dataset after 2012. Because the goal of the study is to refine the analysis of the relationship of SST and TC intensity from Whitney and Hobgood (1997), the consideration of TC climatology in the study coincides with the data availability of the daily SST dataset, covering the period of 1982–2013.

Since only storm data within the ENP boundary, as defined in this study, are of interest for this work, a total of 1445 six-hourly TC observations that lie west of 140°W were eliminated. During the 32-year span, a total of 496 ENP storms were associated with 12,657 six-hourly TC observations, approximately 25.5 six-hourly observations per TC. In comparison, an average of 24.1 six-hourly observations are associated with each storm during the 1963–1993 period from Whitney and Hobgood (1997), a slightly shorter storm duration per TC than the analysis period of the study. Of the 1445 ENP storm observations eliminated beyond 140°W, 84 of them had continued to track further westward, past the International Date Line.

Daily mean SST values are retrieved from Optimum Interpolation SST dataset from the National Oceanic and Atmospheric Administration/National Climatic Data Center (NOAA/NCDC) with a spatial resolution of 0.25° by 0.25°.[1] This refined spatial-temporal resolution of SST record had been applied to investigate the TC-induced SST response (Hart et al. 2007; Dare and McBride 2011a) but has not been applied to update the relationship of ENP TC intensity with SST. Of the 12,657 six-hourly observations, 188 were observed over land. Hence, SST values over 12,469 TC observations from 1982 to 2013 are matched and extracted based on the linear interpolation of nearby SST grids. Because TCs had been shown to reduce local SST, averages of SST values 1 week prior to and after each storm passage at each TC

---

position are also included to monitor the progression of SST-dependent TC intensity. In total, a time series of 15 days of SSTs are obtained in association with each TC position.

The SST control of the maximum TC intensity has been established by a clear statistical linkage when SST is treated as a continuous variable. However, because there remain uncertainties in the measurement of storm wind speed at the tropical depression stage, records with wind speed below 18 m s^{-1} are often considered unreliable (Collins 2010). While the SST effect at various TC stages is of inherent interest, only maximum wind speeds for named storms (NS, sustained wind speed between 18 and 32 m s^{-1}), hurricanes (H, sustained wind speed between 33 and 50 m s^{-1}) and major hurricanes (MH, sustained wind speed greater than 50 m s^{-1}) are quantitatively related to the underlying seawater temperature. Any TC observation over land is of necessity associated with missing SST data. Consequently, a total of 188 observations and 2 storms that had their maximum lifetime intensities detected onshore are removed from the correlation analysis.

To update the previous Eastern Pacific Maximum Potential Intensity developed over the 1963–1993 period (Whitney and Hobgood 1997), all TC tracks are binned into a total of 13 SST groups from 19 to 31 °C, each with a 1 °C range. As an alternative way to demonstrate the impact of SST on TC intensity, daily SSTs 7 days prior to storm arrivals were averaged and rounded to the nearest whole number. As evidence of local SST warming, additional storm intensity data at the 30 °C and 31 °C SST categories are included in our analysis and added from a range of 19 to 29 °C groups (at the 1 °C SST interval) during the 1963–1993 TC climatological record (Whitney and Hobgood 1997). The maximum intensity values at each SST group are extracted to develop an empirical function that best fit these data points. Results were repeated for each of the ENP Main Development Region (MDR) subdivisions. Due to a lack of data for SST groups below 19 °C (23 °C), 27 (16) observations were removed from WDR (EDR).

To further understand the longitudinal variation of ENP storm activity and how TC intensity would respond to SST differences, the TC track record is longitudinally binned into subdivisions of the MDR: EDR and WDR (Fig. 3.1). The regional
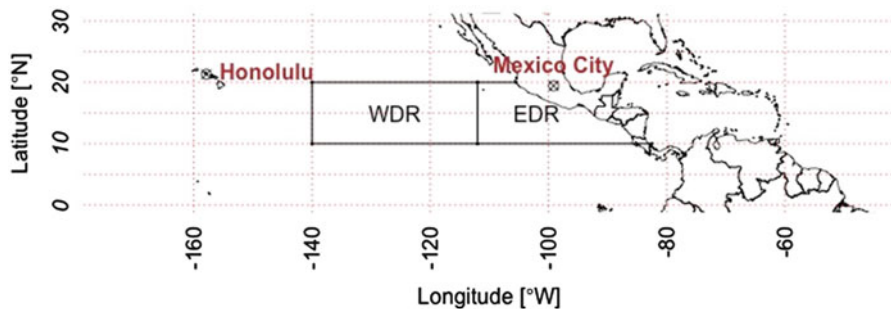

Fig. 3.1 The subdivision of the ENP Main Development Region (MDR) into the EDR and WDR

affiliation of each storm is directly linked to the region where a storm's maximum intensity is achieved (Collins and Roache 2011). For example, if a storm is formed in EDR but attained its maximum intensity in WDR, it is considered as a WDR storm. Additionally, for Sects. 5, 6 and 7, storm observations are partitioned into EDR or WDR according to their six-hourly positions, and their intensities are directly related to the underlying SST measurements. To compare with previous analysis performed by Whitney and Hobgood (1997), the relative velocity of storm track is compiled and calculated by subtracting its translation speed from the maximum wind speed. Translation speed is calculated by dividing the total distance travelled 6 h before and after the storm's current position, except at the initiation and dissipation points where six-hourly movements between the first two points and last two points are computed respectively (DeMaria and Kaplan 1994; Whitney and Hobgood 1997; Mei et al. 2012). The average translation speed for 12,657 tracks is about 4.4 m s^{-1}, comparable to the value of 4.7 m s^{-1}, noted in Whitney and Hobgood (1997).

3 Longitudinal Division of ENP Basin

Of the 496 ENP storms identified, many did not remain within the region where they first formed. Table 3.1 shows that if storms are regionally separated based on locations where they were originally detected, more than three quarters of seasonal storm counts were derived from EDR. However, many had achieved their maximum winds and spent the majority of their lifespan after entering the WDR. During this type of transition, others have suggested that these EDR-originated systems should be designated as WDR storms (Collins and Mason 2000; Collins and Roache 2011). As such, there tends to be a greater number of WDR storms produced during any storm season within a given annual cycle. Of the total 496 ENP storms between 1982 and 2013, the EDR-to-WDR storm ratio is approximately 3:4. In other words, a net movement of EDR-originated storms into WDR occurs every season. Although it

Table 3.1 Annual/seasonal numbers of storm genesis in terms of named/tropical storms (NS), hurricanes (H) and major hurricanes (MH) are stratified between EDR and WDR averaged from 1982 to 2013 based on the location where the peak intensity is established. Total storm count is also sorted according to where storms were initially detected

	EDR	WDR
Initial	11.8	3.8
NS	6.7	8.8
H	3.6	5.0
MH	3.0	5.6

is much more common for WDR storms to originate from the EDR, Rosa (1994) is the only exception where its region of translocation is reversed. Rosa (1994) originated in the WDR and unconventionally migrated to the EDR, where it peaked as a Category 2 (wind speed greater than 42.7 m s^{-1}) storm prior to dissipation over Mexico.

When the six-hourly TC observations are regionally assigned to where each of the 496 ENP storms attained its maximum lifetime intensity, TCs that tracked beyond 140°W are also included. Of all six-hourly track records associated with WDR storms, only 19 out of 8679 WDR storm tracks are recorded to have reached land. In comparison, a greater proportion (170 out of 5425) of EDR storm track points made landfall. While WDR storms are generally expected to travel westward, sometimes passing over Hawaii, only one had crossed Hawaii. This is due to a combination of the fact that Hawaii has a smaller land surface and that most of WDR storm landfalls on the North American continent require westerly winds to induce strong TC recurvature. Interestingly, when comparing the average translational speed between EDR and WDR landfalling storms, significant differences were detected. The average translation speed (15.3 m s^{-1}) associated with these EDR landfalling storm records is almost twice as large as the average (7.4 m s^{-1}) of all landfalling WDR storm tracks. Part of the difference is due to an overall more rapid recurvature of EDR storms when making landfalls.

During the period of 1982–2013, the annual average number of ENP storm count has been decreasing. This is mostly attributed to a below-normal number of WDR storms. On the other hand, the number of EDR storms stays relatively the same. Using the Theil-Sen slope estimator, a reduction of 0.17 WDR storms per year (5.3 storms over 32 years) is observed to be statistically significant at the 5 % significance level (Fig. 3.2). This value is large considering the seasonal average of storm count is 8.8 storms in the region. Since WDR storm activity represents a significant proportion of ENP storm activity, this reduction of WDR storm count is a major contributor to a decreasing trend (significant at $p < 0.05$, not shown) of total ENP storms during the same time period.

During an average hurricane season, more than half of the total ENP storm count (15.5) became WDR storms. However, the most recent (1981–2013) TC climatology indicates that the number of EDR-originated WDR storms has diminished. Trend analysis shows the annual proportion of these transitioning WDR storms to the total ENP storm count has decreased significantly ($p < 0.05$) averaging to a reduction of 5.1 WDR storms over the time period (Fig. 3.3). In addition, the reduced WDR storms match well with the diminishing number of EDR-to-WDR storms. As such, this downward trend implies seasonal WDR storm frequency is becoming less reliant on EDR for storm initiations, leading to further storm growth and development in the WDR.

While a reduced number of WDR storms may seem that WDR storm seasons are progressively less active, it should be interpreted more carefully. Most of the downward trend of total WDR storm (Fig. 3.2) is explained by the lack of transfer
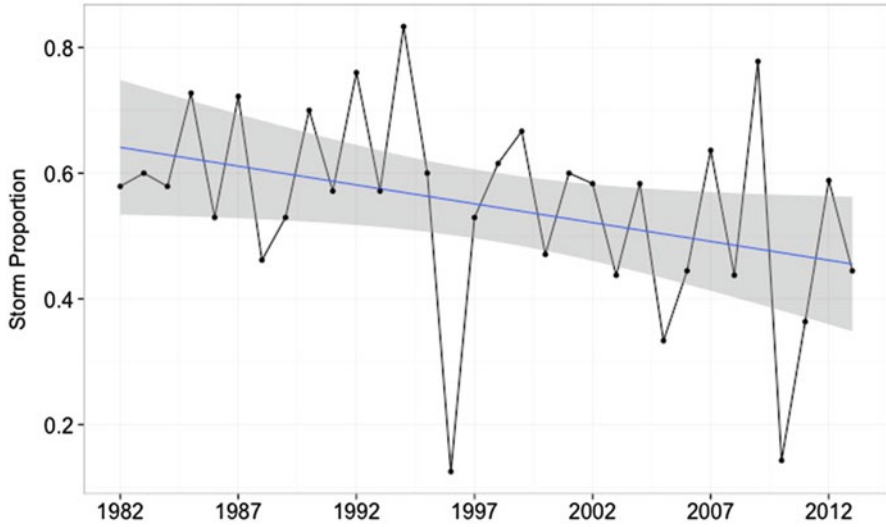
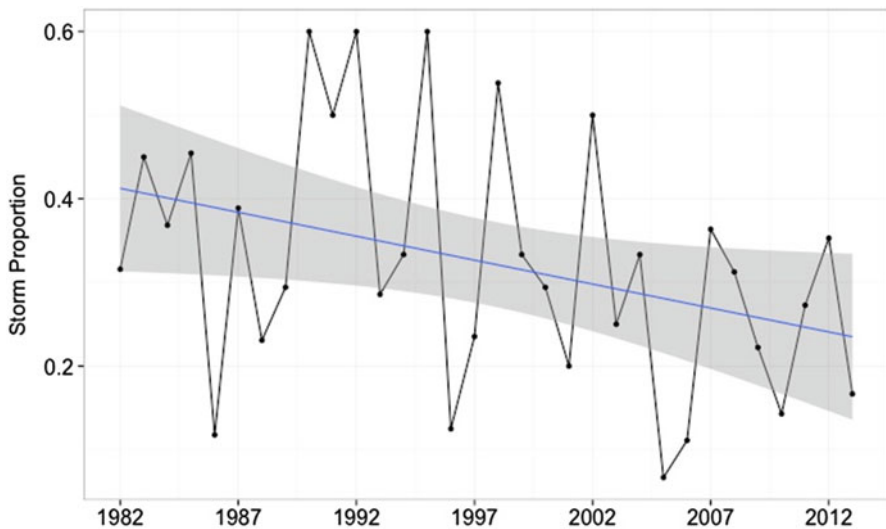**Fig. 3.2** Annual proportions of WDR storms to all ENP storms from 1982 to 2013

Fig. 3.3 Annual proportions of EDR-derived WDR storms to the total WDR storm count from 1982 to 2013

of storms from the EDR to WDR (Fig. 3.3). At the same time, the number of WDR storms that originated within the WDR boundary has remained stable. In fact, numbers of WDR hurricanes and major hurricanes have both increased significantly (Collins and Mason 2000).

4 Displacements of Maximum TC Intensity and Maximum SST and Initial Genesis Point

Under the influence of tropical easterly flow, ENP storms predominantly track westward and gradually divert poleward, over cooler tropical water prior to dissipation. Many of them can be traced as far upstream as African easterly waves that only intensify to TC strength after crossing the North Atlantic, the Caribbean Sea and the Gulf of Mexico (Molinari et al. 1997; Thorncroft and Hodges 2001). While most storms form close to the North American coast, these storms typically undergo intensification and obtain their maximum lifetime intensity distant from the coast. Figures 3.4a, b show the northwest tendency for storms before gaining peak intensity. On average, it requires a storm to shift 3.7° northward and 9.6° westward of its original identification point to achieve its maximum lifetime wind speed.
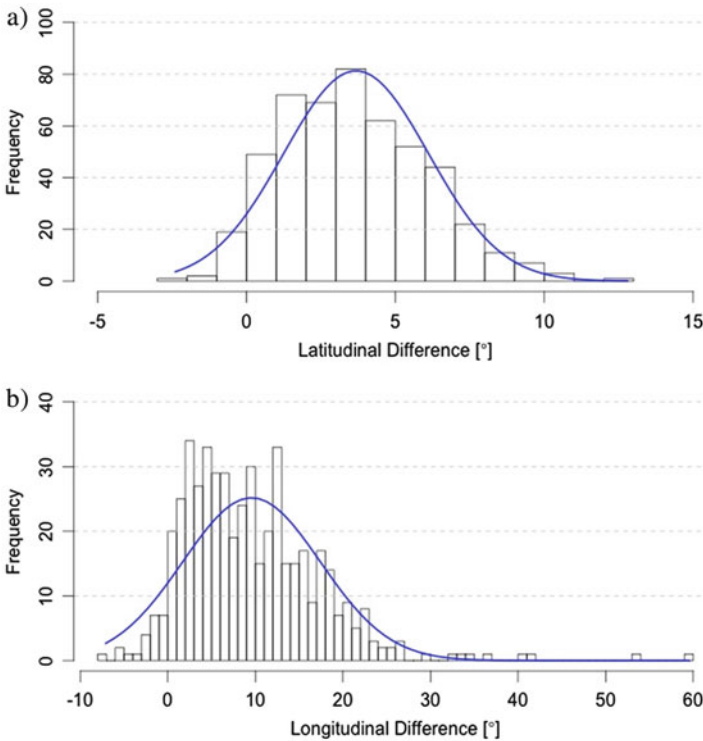

Fig. 3.4 (**a**) Distribution of latitudinal differences between the locations of storm genesis and maximum lifetime intensity for all ENP storms from 1982 to 2013 and (**b**) same as (**a**), but for longitudinal differences. Each histogram is outlined with a normal curve (in *blue*)
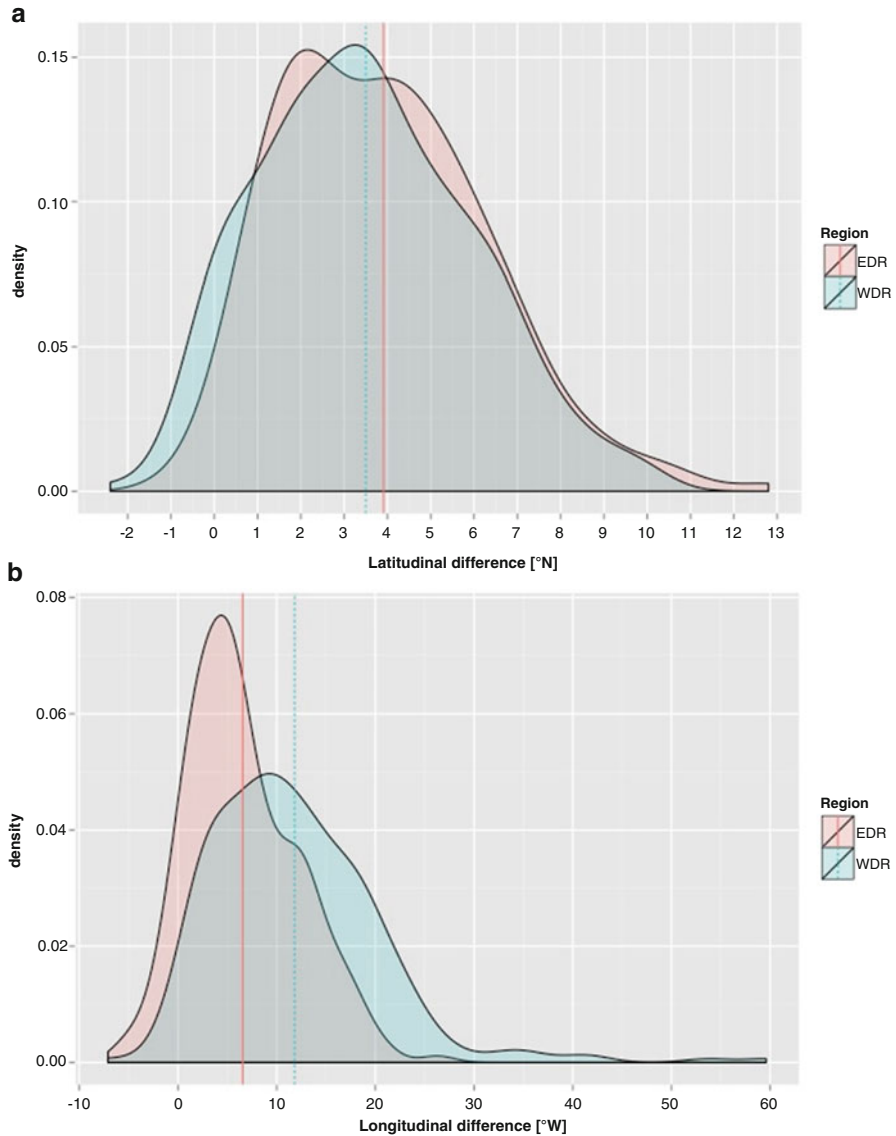
Fig. 3.5 (**a**) Distribution of latitudinal differences of locations between storm genesis and maximum lifetime intensity for EDR and WDR storms from 1982 to 2013 and (**b**) same as (**a**), but for longitudinal differences

When storms are separated into EDR and WDR subregions, regional variations of latitudinal (Fig.3.5a) and longitudinal (Fig. 3.5b) differences are observed despite the average locations of their maximum lifetime intensities being found northwest of their initial detections. While the mean latitudinal difference between the initial storm detection and its maximum intensity of EDR storms is only 0.4° northward

of WDR storms, WDR storms' mean longitudinal difference is 5.3° westward of EDR storms. Although a greater longitudinal shift is detected for WDR storms, it is mostly attributed to the fact that 58 % of WDR storms were initiated in the EDR and experienced longer periods of intensification than those WDR storms that were originated within WDR. However, even if WDR storms that originated from EDR are removed, WDR's mean longitudinal difference is still maintained at 2.4° greater, significant at the 5 % confidence interval, than that of EDR storm's average longitudinal shift. The ability for WDR storms to track over a greater distance before achieving maximum intensity is linked to a longer longitudinal shift. This is supported by a clear right-tailed distribution for longitudinal differences, mainly attributed to WDR storms (Fig. 3.5b).

Although ocean temperature tends to be higher where storms initially formed, their genesis locations are not necessarily the highest SST experienced during a storm's lifecycle. The higher SST tends to provide the most optimum condition for TC development. However, its maximum lifetime intensity is rarely achieved where the highest SST is encountered. On average, the maximum intensity is located north-west of where the highest weekly SST is found a week prior to the storm passage. The resulting latitudinal (Fig. 3.6a) and longitudinal (Fig. 3.6b) differences are more evenly distributed compared to displacements between maximum intensity and initial storm genesis location (Fig. 3.4a, b). Such a comparison also demonstrates that the highest SSTs are experienced closer to maximum lifetime intensities than initial genesis locations of ENP storms. An average delay of 1.7 days is observed for a storm to establish peak intensity after experiencing its warmest seawater versus approximately 3 days after a storm was first generated. This coincidence where the highest storm intensity is matched with the highest SST was found for only 18 storms, representing less than 4 % of the total storm count.

The spatial misalignment of maximum SST and maximum intensity is generally displayed by North Atlantic storms though the extent of displacement differs compared to ENP storms. While two-thirds of North Atlantic storms met their maximum SSTs within 5° latitude of maximum lifetime intensity (Michaels et al. 2006), 83 % of ENP storms had done so. Overall, this latitudinal displacement for ENP storms' maximum intensity is 2.2° northward of where maximum SST is achieved, only half of North Atlantic storms' displacement (Michaels et al. 2006). These comparisons relative to North Atlantic storms signify ENP storms' stronger linkage to areas with the highest SST in acquiring maximum intensity.

For storms that took an eastward recurvature or landfall, the highest SSTs are often found near shore when their strengths are diminishing, possibly in conjunction with extratropical transitioning. Interestingly, peak intensities for these storms took less time to establish than those that experience warmest SST at their earliest stage of development. As contrasting environmental conditions near shore and in the open water could dictate a difference of TC development, the WDR reveals a strong longitudinal displacement (Fig. 3.7b) between locations of the warmest SST and maximum lifetime intensity (Fig. 3.7a). Although this could also be attributed to WDR storms that have encountered the maximum SST while they were still in the EDR, 137 (or 40 %) of WDR storms match this criterion. This is lower than
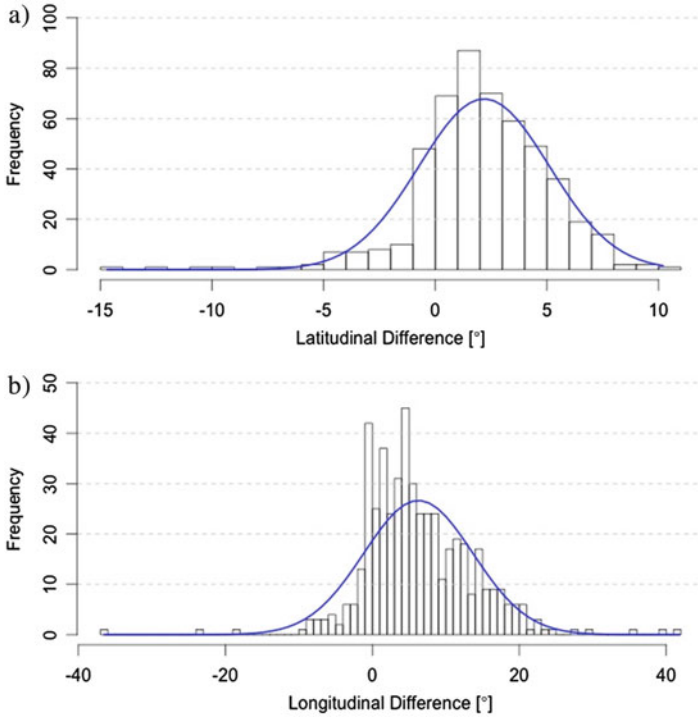
Fig. 3.6 (**a**) Distribution of latitudinal differences between the locations of maximum SST and maximum lifetime intensity for all ENP storms from 1982 to 2013 and (**b**) same as (**a**), but for longitudinal differences. Each histogram is outlined with a normal curve (in *blue*)

those storms (58 %) that formed in EDR but achieved maximum lifetime intensities in WDR. Even when these storms are excluded, storms that attained maximum intensity and maximum SST in the WDR still maintain a 2° westward bias over EDR storms.

5 Correlation Between SST and TC Intensity

5.1 All Observations

Since the onset of a storm induces a cold wake (due to turbulence-induced entrainment below surface waters) and thus obscures the SST-TC intensity relationship, a 7-day SST average prior to the storm arrival was used to correlate with the intensity observations. Possibly due to a large sample size ($n = 12,469$), Fig. 3.8 shows the linear regression fit is significant ($p < 0.001$) despite a slope of 0.889 and R^2 value of 0.020 for storm track positions observed prior to crossing the westernmost boundary
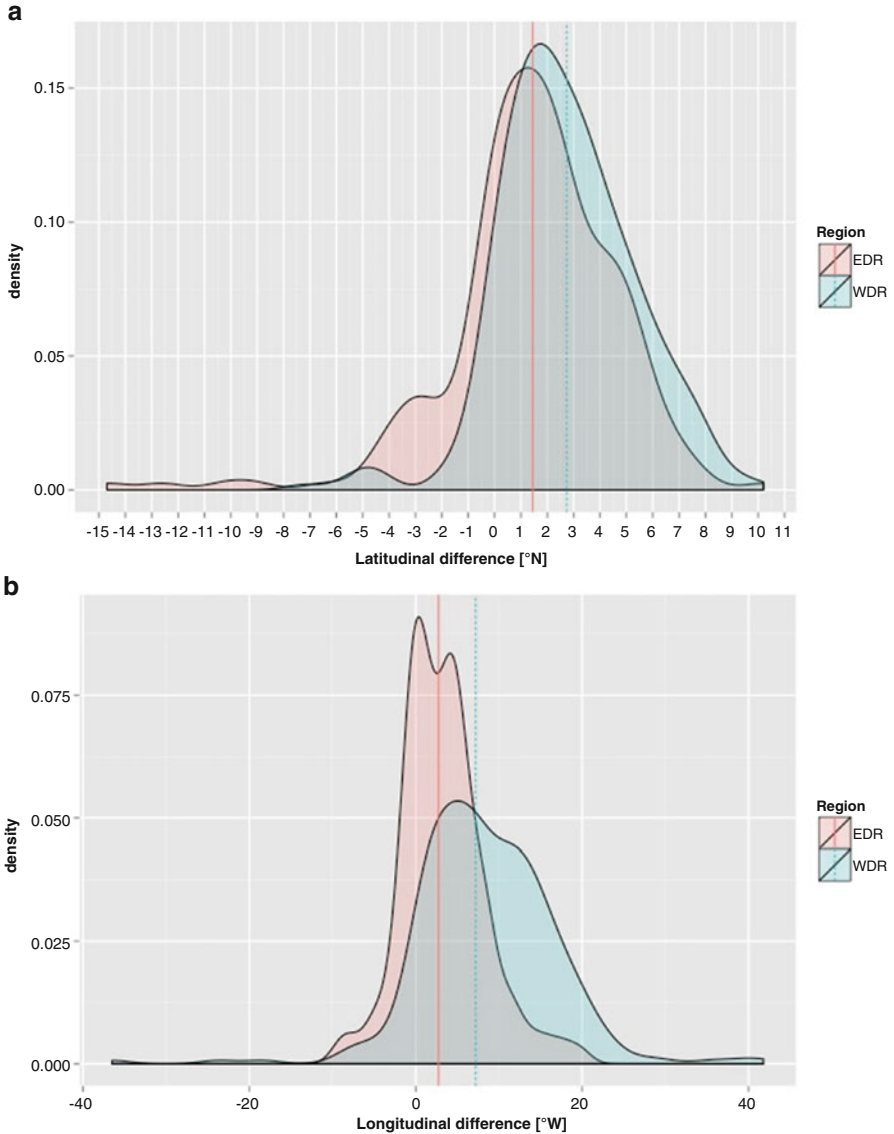
Fig. 3.7 (**a**) Distribution of latitudinal differences between locations of maximum SST and maximum lifetime intensity for EDR and WDR storms from 1982 to 2013 and (**b**) same as (**a**), but for longitudinal differences

division at 140°W. Such a low value for the coefficient of determination implies that SST is a rather weak predictor for storm intensity.

Though the explained variance is small, yet significant, it is higher than a similar correlation analysis performed in the North Atlantic basin (Michaels et al. 2006).
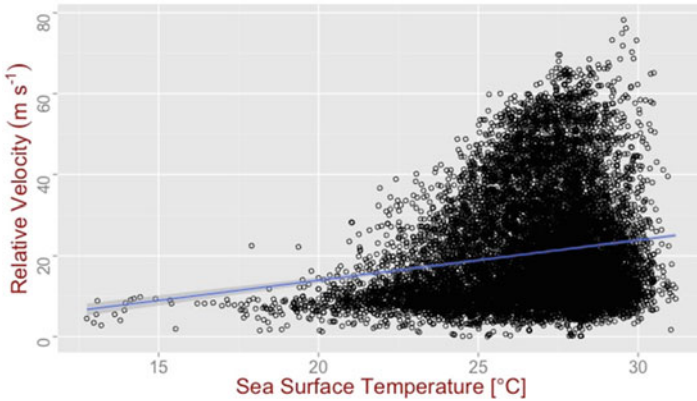
Fig. 3.8 Scatterplot and regression fit for all observations of TC intensity against the weekly SSTs averaged over 7 days prior to storm passage

If storm tracks that traversed west of the ENP boundary are also included (not shown), the linear regression is still significant. Such a significant linkage between SST and TC intensity is consistent with that of Ralph and Gough (2009), which considered the correlation of TC activity of all storm strengths and basin-wide SSTs at a monthly scale. Although our analysis shows that the explained variance is small, this association of near-time SSTs and TC wind speeds is consistent with Michaels et al. (2006). Though SST certainly provides a certain degree of influence on the upper bound of TC intensity, SST is clearly far from being the sole control of TC intensity. Even when elevated SSTs are observed, other atmospheric factors such as wind shear diminish TC strength (Landsea et al. 1998; Maue 2009). The fact that the R^2 in the present study is higher than a similar analysis conducted for North Atlantic storms (Michaels et al. 2006) may indicate greater SST influences on ENP storm intensities.

Upon investigating how TC intensity is related to SST at a daily scale, the temperature measurement at the ocean surface demonstrates a two-way, SST-TC relationship. Though it is shown in Fig. 3.8 that SST directly contributes to TC intensification, storm passage is capable of cooling the ocean surface at least a week prior to its arrival. The strength of SST reduction depends on storm translation speed and its intensity (Cione and Uhlhorn 2003; Mei and Pasquero 2013). For instance, a slow-moving storm with high winds would likely enhance the process of vertical mixing by drawing cold water underneath. The result of this cold wake left behind a TC may impede its own development and impose a negative impact on the formation and development of potential storms nearby (Bender and Ginis 2000).

Figure 3.9 shows the SST averages 7 days before and after (total of 15 days) for locations of all 12,469 storm tracks. Generally, this cooling remained for at least 1 week since the storm has departed, with the greatest SST reduction experienced during the period between 1 day before onset until the day of storm arrival. Such a sharp drop in the ocean surface temperature is likely the result of a greater
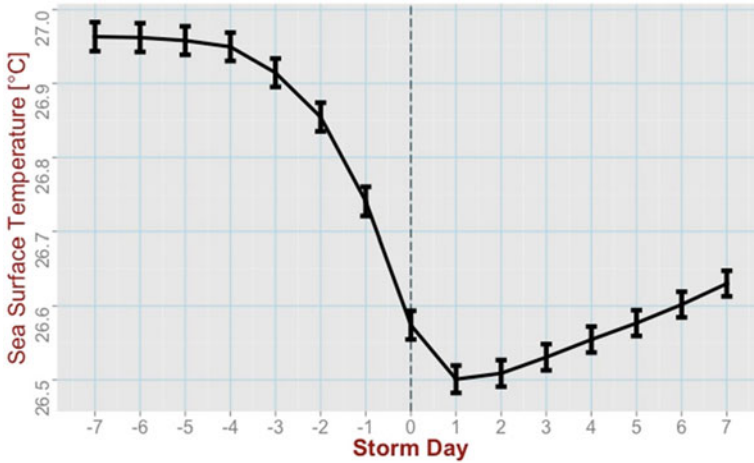
Fig. 3.9 Daily SST response (with standard error) to the influence of storm passage over a 15-day time series

vertical mixing due to a close proximity to the radius of maximum winds and storm movement, which entrains cooler waters beneath the sea surface. Such a cooling effect lasts longer and is more pronounced for locations that experience storms with lower translation speeds and higher storm intensities (Dare and McBride 2011a). Compared to the North Atlantic TCs, since the average translation speed is higher in that basin, SST reduction associated with a slower storm movement is generally greater in the ENP basin.

When all 12,469 observations of storm intensity are correlated with their same-day SSTs (i.e. Day 0), a weak relationship is found (slope = 0.63078 and $R^2 = 0.01094$). Although the result of a linear least-squares fit maintains its statistical significance ($p < 0.001$), the fact that the greatest SST decrease occurs during the day prior to storm arrival weakens the near-time SST-TC intensity relationship. The effect of SST cooling on the SST-TC intensity relationship is likely to be most important when storms are undergoing rapid intensification, particular during September, the peak month of the ENP hurricane season (Kaplan et al. 2010). Once the TC-induced rate of SST cooling diminishes, storms are found to intensify at a faster rate (Cione and Uhlhorn 2003).

While the choice of daily SST at least a week before storm arrival does not dramatically change the explained variance for the linear fit with TC intensity (Table 3.2), the use of the weekly SST dataset (Michaels et al. 2006) may not be as closely aligned to the initial storm detection as the daily time interval data. For instance, when a storm has just formed, the SSTs averaged during the past week may be more critical at determining storm genesis than TC intensification. Figure 3.10 compares a 15-day time series of SST averages centred at the genesis stage and the time when a storm's peak intensity is observed. From the day before until the day after the detection of maximum lifetime intensity, the most dramatic SST decline

Table 3.2 Regression analysis of storm intensity of all EDR and WDR observations with daily SST at 7 days prior to storm passage with Day 0 being the arrival day of storm passage

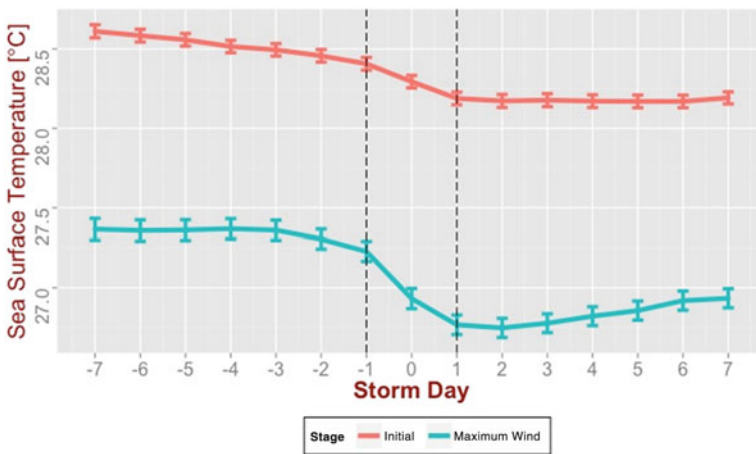| Region/days before	EDR		WDR	
	Slope	R^2	Slope	R^2
7	−0.79	0.01	1.55	0.06
6	−0.81	0.01	1.56	0.06
5	−0.72	0.00	1.60	0.06
4	−0.67	0.00	1.61	0.06
3	−0.69	0.00	1.60	0.06
2	−0.67	0.00	1.62	0.06
1	−0.63	0.00	1.59	0.06
0	−1.43	0.02	1.32	0.04
7-day average	−0.79	0.00	1.64	0.06

Fig. 3.10 Same as in Fig. 3.9, but the 15-day SST is centred around the storm genesis and maximum lifetime TC intensity. *Dashed lines* represent the daily range of the highest rate of SST reduction

can be discerned. This is mostly likely due to a combination of a slower translation speed and a strong TC wind speed in churning up colder water from below (Mei and Pasquero 2013). Since weak TC winds are associated with fast-moving, decaying storms, virtually little to no SST recovery is observed past the storm genesis stage. In contrast, the average SST recovery at only those locations that just experienced peak storm intensities is 0.06 °C higher than the average of all TC observations.

5.2   MDR Subdivisions

When TC observations are subdivided and binned into EDR and WDR, the sensitivity of TC intensity to SST is regionally distinct. With the addition of a
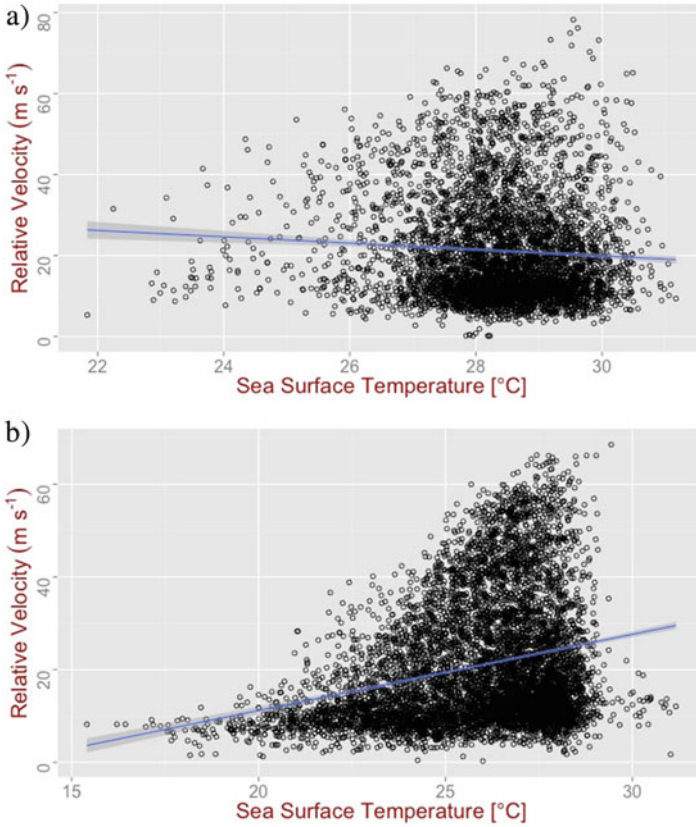
Fig. 3.11 (**a**) Relative wind speeds for all EDR storm observations and (**b**) same as (**a**) but for all WDR storm observations

linear regression of least-squares fit, Fig. 3.11a, b shows a scatterplot of EDR (WDR) storm intensity and SST averaged over a 7-day period prior to TC detection. Compared to EDR, despite a rather low explained variance, WDR storm intensities are more responsive to SST differences. In fact, the slope is nearly twice as large for MDR storms during any day of the week prior to the TC arrival. From Table 3.2, the worst fit is found at Day 0, when the negative (positive) slope is strongest (weakest) at EDR (WDR). In the EDR, this corresponds to the time when the greatest rate of SST reduction due to storm influences is observed (Fig. 3.12). This SST reduction in EDR continues until a local minimum is observed 2 days after the storm appearance. While the temperature of the ocean surface is noted to reduce at a slower pace a week prior until the day before EDR storms arrive, SST is observed to start cooling only 4 days prior to TC arrival until the local minimum appears the day after the WDR storm passage.
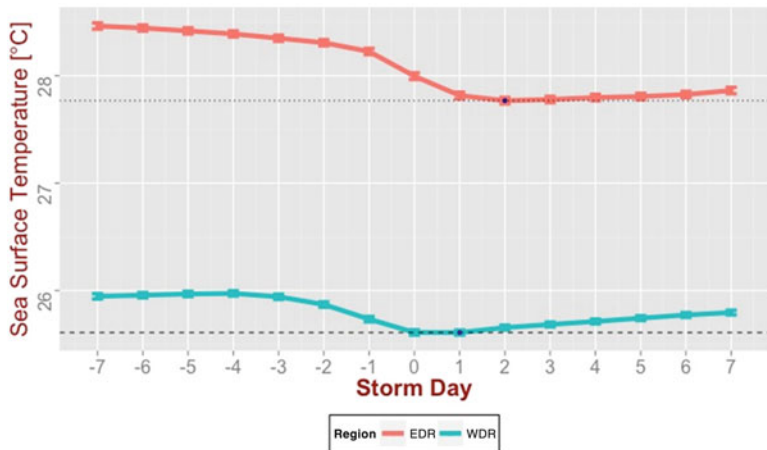
Fig. 3.12 Same as Fig. 3.9, but separated for storm passages of EDR and WDR observations. *Dashed lines* represent the reference SSTs of local minima over for EDR and WDR

Subdividing ENP storm observations into EDR and WDR sectors is also critically important to the understanding of the regional difference in which TC wind speed responds to SSTs at different storm development stages. In particular, the relationship of WDR storm intensity with the underlying SST shows a greater significance when the maximum lifetime intensity is examined. Such a finding of SST control over the maximum lifetime TC intensity would not have been possible if the ENP basin had not been subdivided. Similar to the above result, little association with SST is detected on the day when maximum relative wind is detected. On average, the greatest correlations are observed 2 days before TC arrivals when the impact of TCs on ocean temperature is less pronounced. This observation has been previously hypothesized but not proven until the use of the daily SST dataset. In terms of ocean surface cooling, EDR storm observations generate greater SST reductions at least a week prior to storm geneses and the attainment of maximum intensities; however, TC passages at both regions display little evidence of SST recoveries (Figs. 3.13a, b). However, dramatic differences of SST responses between EDR and WDR are noticed for locations that experience passages of maximum lifetime intensities (Fig. 3.13b). EDR storm records tend to be accompanied by greater SST reduction than WDRs.

Regional sensitivity for the maximum lifetime intensity to SSTs is found to differ between EDR and WDR storms. Figure 3.14a, b depicts the scatterplots of maximum lifetime intensity of relative winds with average weekly SSTs, 7 days prior to TC arrival for all 283 (213) WDR (EDR) storms. Comparatively, the SST range when WDR major hurricanes (Fig. 3.14a) have established peak intensities is shorter, and on average colder, than that of EDR major hurricanes (Fig. 3.14b). Specifically, this study found the importance of an SST of 25 °C (24 °C), above which all but one major hurricane (hurricanes) has established peak intensities in
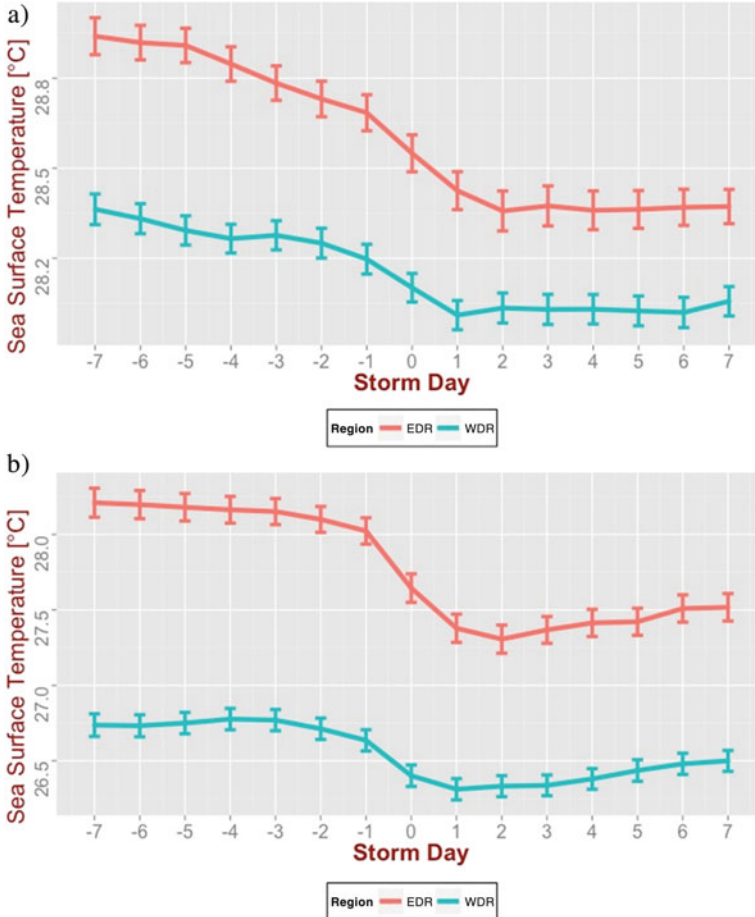
Fig. 3.13 (**a**) Same as Fig. 3.12, but for the average SST conditions during storm genesis and (**b**) same as (**a**) but during the maximum lifetime intensity

WDR. Meanwhile, such SST limitation is less clear in EDR, with most of its major hurricanes established at SSTs higher than 27 °C. Compared to the maximum SST level of 28.25 °C that is required to attain the maximum lifetime intensity of North Atlantic major hurricanes (Michaels et al. 2006), this SST requirement in WDR is dramatically lower. Comparison studies within and between major TC development basins suggest the SST requirement to sustain major hurricanes is not uniform.

Although an SST threshold of 28.25 °C is identified for North Atlantic storms to achieve maximum strengths of major hurricane status, Michaels et al. (2006) show North Atlantic TC winds that achieved maximum intensities past this SST requirement have little to no relationship with corresponding SSTs. Even if only the intensities of major hurricanes were investigated, SST does not seem to be the
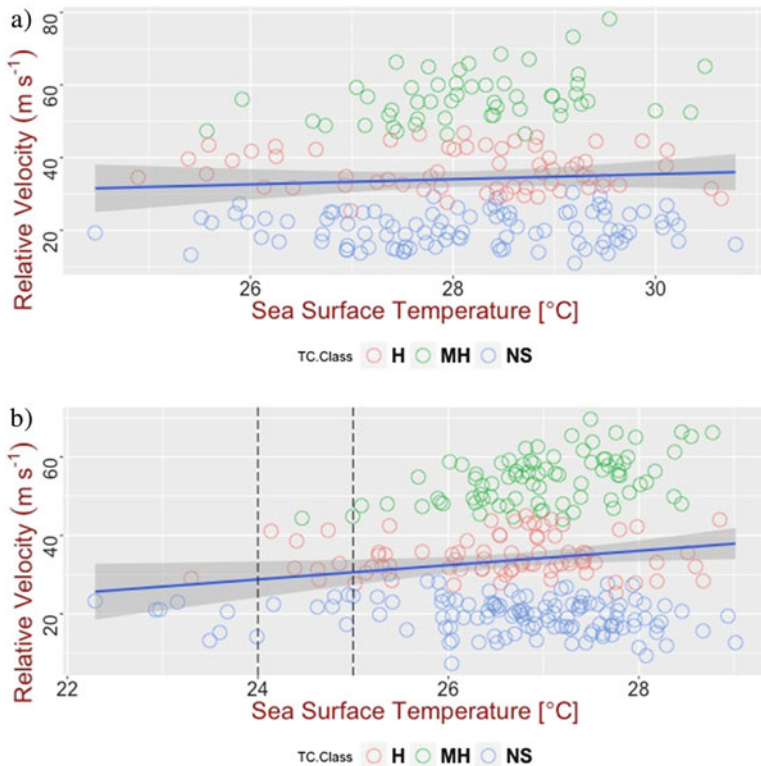
Fig. 3.14 (**a**) Scatterplot and linear regression of maximum lifetime intensity of relative velocity for EDR storms ($N = 213$) and daily SSTs averaged a week prior to maximum storm strength and (**b**) same as (**a**) but for WDR storms ($N = 283$). The *dashed lines* with cooler (warmer) SST indicates the requirement for hurricane (major hurricane) genesis

overriding factor in determining the maximum TC winds. However, in the ENP basin, the maximum intensity of WDR major hurricanes demonstrates significant relationship with daily SSTs. Figure 3.15 shows the SST and TC intensity for WDR major hurricanes 3 days before relative winds are achieved. A linear regression analysis on this day has the highest slope and explained variance. To compare with the previous result shown in the North Atlantic basin (Michaels et al. 2006), this correlation test was also replicated using maximum winds (relative velocity + translation speed); and, the result also shows similar statistical significance at $p < 0.01$. Though maximum intensities of WDR major hurricanes are critically dependent on SST conditions, many WDR storms remain weakly developed despite encountering favourable SST conditions that are well above the minimum requirement (25 °C) to attain the maximum strength of major hurricanes. In contrast, while maximum lifetime TC intensity for all EDR storms is not found to positively correlate with ocean surface temperature, a weak, but positive, relationship was found for maximum winds of EDR major hurricanes and their underlying SSTs.
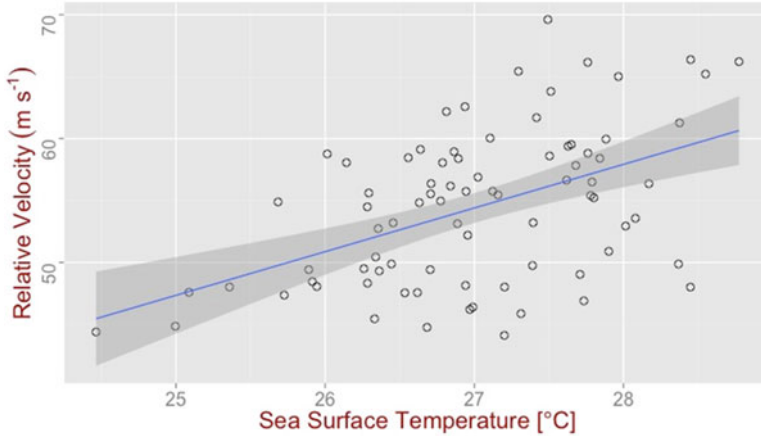
Fig. 3.15 Scatterplot and linear regression of maximum lifetime intensity of relative velocity for WDR storms that reached major hurricane strength with SST 3 days before maximum storm strength

6   Upper Bound of TC Intensity by SST Groups

In addition to statistically linking SSTs to observations of TC winds, the impact of increasing SST on the maximum sustained winds can also be explored by stratifying records of TC wind speed into SST groups based on the work of DeMaria and Kaplan (1994). By rounding average SST values a week prior to TC arrival to the nearest integer, TC winds have generally maintained the same relationship with increasing SSTs as found by Whitney and Hobgood (1997). Overall, warmer SSTs are able to sustain a higher maximum TC intensity. Compared with Whitney and Hobgood (1997), an update to the current TC record shows that the maximum intensities at some of the highest SST categories are increasing.

Table 3.3 summarizes the 1982–2013 storm intensities in each SST bin, updated from 1963 to 1993 climatology (Whitney and Hobgood 1997). Two extra (30 °C and 31 °C) SST bins are now required, though it has been noted that there were few storm observations from 1963 to 1993 climatology that encounter SSTs greater than 29.5 °C. Similar proportions (77 %) of the total TC intensity observations were found in the 26 °C or higher SST bins, though the highest average TC intensity has shifted from 26 °C (Whitney and Hobgood 1997) to 27 °C bin (Table 3.3). A gradual decrease in the average TC intensity with increasing SST is partly due to degrading storms recurring over shallow and warm water prior to dissipation at landfall. It could be also attributed to a tendency for storms to form and develop over the highest SSTs and slowly decay while passing over cooler water (Whitney and Hobgood 1997).

Though the total number of analysis years is 1 year more than that of Whitney and Hobgood (1997), there are an additional 1595 SST observations associated

Table 3.3 Summary of TC intensity records stratified into SST bins

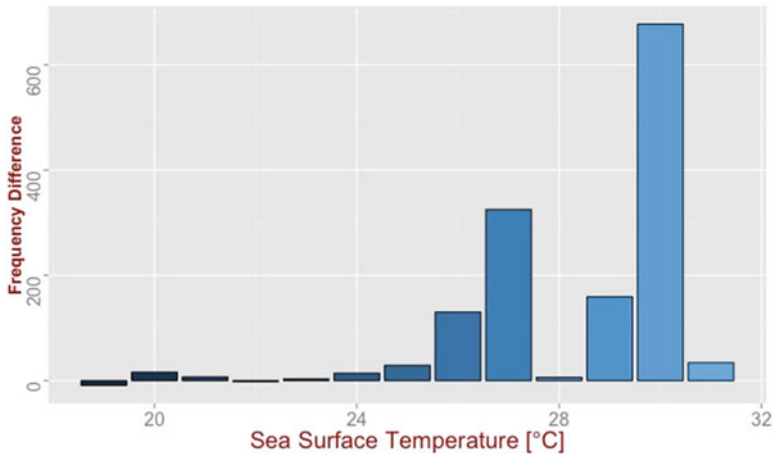| SST (°C)	Sample size	Average intensity (m s^{-1})	Maximum intensity (m s^{-1})
19.0	34	7.4	12.2
20.0	74	8.5	16.2
21.0	148	10.2	28.3
22.0	280	12.2	38.8
23.0	475	13.8	40.1
24.0	714	16.4	48.7
25.0	952	21.6	55.7
26.0	1,386	24.4	60.0
27.0	2,367	24.4	66.3
28.0	3,304	21.4	68.5
29.0	1,966	20.4	74.9
30.0	708	20.1	78.2
31.0	34	18.6	50.4

Fig. 3.16 Anomaly of TC observations in each SST bin during 1982–2013 compared to 1963–1993

with the TC record. This value is large considering that the average number of the SST-TC record between 1963 and 1993 per year is 356.8, roughly averaging 36 more observations/year during the 1982–2013 period. Although it is difficult to attribute the recent spurt of TC activity to climate change due to an inconsistent monitoring of TC tracks when compared with data prior to the 1970s, the recent SST warming has shifted the corresponding surge of TC observations towards the distribution with higher SST values. Figure 3.16 shows that most of the surge in TC detection associated with SST warming occurs preferentially in the higher SST bins. Likewise, less of an increase in TC observations are observed to be distributed

Table 3.4 Details on storms that attained the highest relative winds at each SST bin

| SST (°C)	Year	Name	Latitude (°N)	Longitude (°W)	Maximum winds (m s^{-1})	Strength	Relative winds (m s^{-1})	Region
19.0	2001	NARDA	16.3	139.6	15.4	TD	12.2	WDR
20.0	2005	KENNETH	16.5	139.4	23.1	NS	16.2	WDR
21.0	2013	GIL	13.7	138.2	33.4	H	28.3	WDR
22.0	2004	ISIS	16.3	135.7	43.7	H	38.8	WDR
23.0	2008	CRISTINA	14.1	133.7	46.3	H	40.1	WDR
24.0	1995	ADOLPH	17.8	108.8	51.4	MH	48.7	EDR
25.0	2006	EMILIA	30.8	125.2	59.2	MH	55.7	WDR
26.0	1988	CARLOTTA	21.7	123.7	64.3	MH	60.0	WDR
27.0	1984	NORBERT	19.4	116.3	72.0	MH	66.3	WDR
28.0	1998	KENNA	18.3	108.3	74.6	MH	68.5	EDR
29.0	1997	LINDA	17.7	110.3	79.7	MH	74.9	EDR
30.0	1997	LINDA	17.1	109.6	82.3	MH	78.2	EDR
31.0	2009	JIMENA	15.7	105.5	54.0	MH	50.4	EDR
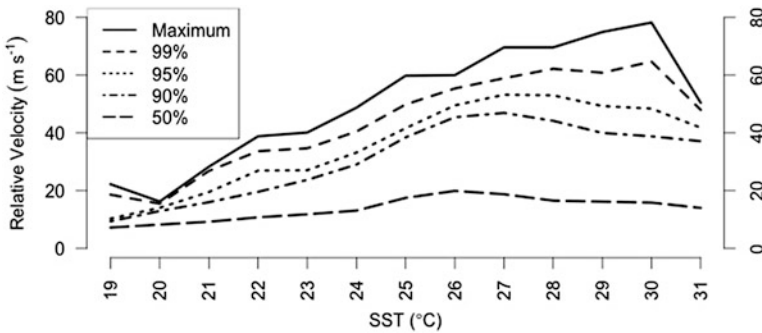
Fig. 3.17 Storm relative winds at the maximum intensity and 99th, 95th, 90th and 50th intensity percentiles at all SST bins after translation speeds have been accounted

at lower SST values. Thus, this improvement of thermodynamic condition is able to allow storms to extract energy to reach higher maximum TC intensities. Consequently, storms (in Table 3.4) that are responsible for achieving the highest maximum intensity in each SST bin differ from those found in Table 3.2 of Whitney and Hobgood (1997). TCs Linda (1997), Kenna (2002) and Rick (2009) had all exceeded the maximum strength of Trudy (1990), which was found to be the most intense storm from an earlier 1963 to 1993 period (Whitney and Hobgood 1997).

Since it is of interest to understand the effect of SSTs on storm intensity, only the maximum, 99th, 95th, 90th and 50th, percentiles of TC winds are plotted in Fig. 3.17. Initial linear increases are noted for 90th percentiles or above though the rate of increase flattens, or even decreases, as bins of higher SSTs are approached. Only the maximum intensity values maintained a linear growth rate with increasing
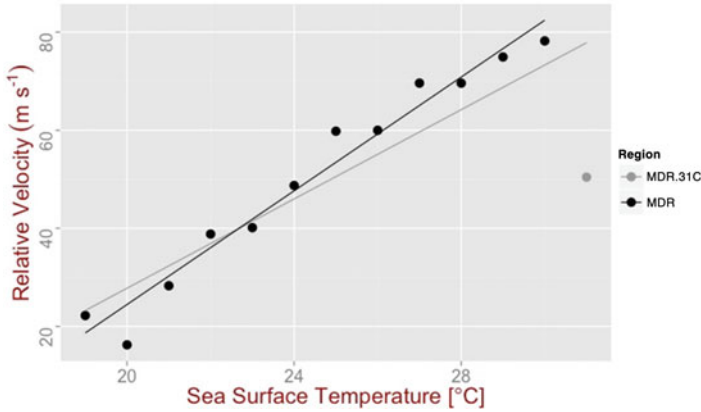
Fig. 3.18 Scatterplot and regression line drawn for the maximum storm intensity attained by each SST bin with and without the maximum intensity at the 31 °C bin

SSTs. Because Fig. 3.18 shows that the maximum intensity dips dramatically at the 31 °C bin, its value is not included in the empirical derivation of MPI (Eq. 3.2), possibly due to a lack of observation in the highest SST category. Using a locally weighted scatterplots smoothing known as LOWESS (not shown), the fit is best described as a linear relationship. The updated (1982–2013) relationship between empirical MPI and SST in the ENP basin has an equation of the form

$$\text{ENPMPI} = A\,(\text{SST}) + B, \tag{3.2}$$

where ENPMPI (m s^{-1}) represents the revised ENP maximum potential intensity, with a constant of $B = -91.4863$ m s^{-1} and a slope of $A = 5.7975$ m s^{-1} °C^{-1}. Overall, 96 % of total data variance is explained by ENPMPI. Compared to Whitney and Hobgood (1997), this updated ENPMPI sees an increase in slope showing the linear fit is stronger than the past TC climatology (Fig. 3.18).

When the ENP MDR is subdivided, it is evident that there are regional differences in the distribution and magnitude of TC intensities among the SST bins. A warmer (colder) SST condition is experienced in the EDR (WDR), where 16 (slightly over a thousand) TC track records are associated with SST bins lower than the 23 °C category (Tables 3.5 and 3.6). Towards the upper bound of TC intensity distribution, over 95 % of EDR storm observations (Table 3.5) are in the 26 °C category or greater, while only 64 % for the WDR (Table 3.6). When the maximum intensity is regionally compared for each SST bin, maximum intensities observed in the WDR are higher at SST categories of 25 °C and 27 °C (Table 3.6), while the highest attained TC intensities at other SST bins are higher in the EDR (Table 3.5). Although maximum TC intensity is not unanimously favoured within a particular ENP MDR subdivision, the average storm intensity at each SST bin is consistently stronger in the EDR (Table 3.5).

Table 3.5 Same as in Table 3.3 but for six-hourly TC observations in EDR

SST (°C) bin	Sample size	Average intensity (m s^{-1})	Maximum intensity (m s^{-1})
<23.5	16	20.9	45.3
24	33	23.6	52.2
25	48	29.1	48.7
26	178	30.2	60.3
27	597	27.8	62.7
28	1,728	22.3	73.3
29	1,714	18.1	78.2
30	685	16.7	62.2
31	27	13.3	33.1

Table 3.6 Same as in Table 3.3 but for six-hourly TC observations in WDR

SST (°C) bin	Sample size	Average intensity (m s^{-1})	Maximum intensity (m s^{-1})
<18.5	27	6.9	11.8
19	34	7.4	12.2
20	74	8.5	16.2
21	148	10.2	28.3
22	278	12.1	38.8
23	461	13.8	40.1
24	681	16.1	45.2
25	904	21.4	55.7
26	1,208	23.2	60.0
27	1,770	24.6	66.5
28	1,576	24.3	66.2
29	252	21.2	68.7
30	23	12.0	21.9
31	7	10.7	13.7

When maximum, 99th, 95th, 90th and 50th, percentiles of TC intensity are plotted for the EDR (Fig. 3.19a) and WDR (Fig. 3.19b), regionally specific positive relationships are observed for TC intensities. In the EDR, a smoother increase in the maximum TC intensity (1.7 m s^{-1} per °C) is observed while the average WDR intensity experiences a steeper (5.6 m s^{-1} per °C) increase. At TC intensities of lower percentiles, this increase is slower towards the higher SST categories for both regions. When the average intensity within each SST bin is compared between regions, observations from both regions show less sensitivity to higher SST conditions than the maximum intensity. Differences between the two regions are dramatically different for TC winds at the higher percentiles. WDR storm intensities greater than the 90th percentile of each SST bin are more dependent on SSTs than for EDR storms.

Since the ENP basin exhibits longitudinally different SST conditions for TC development, ENPMPI derived above might not best represent the upper limit of
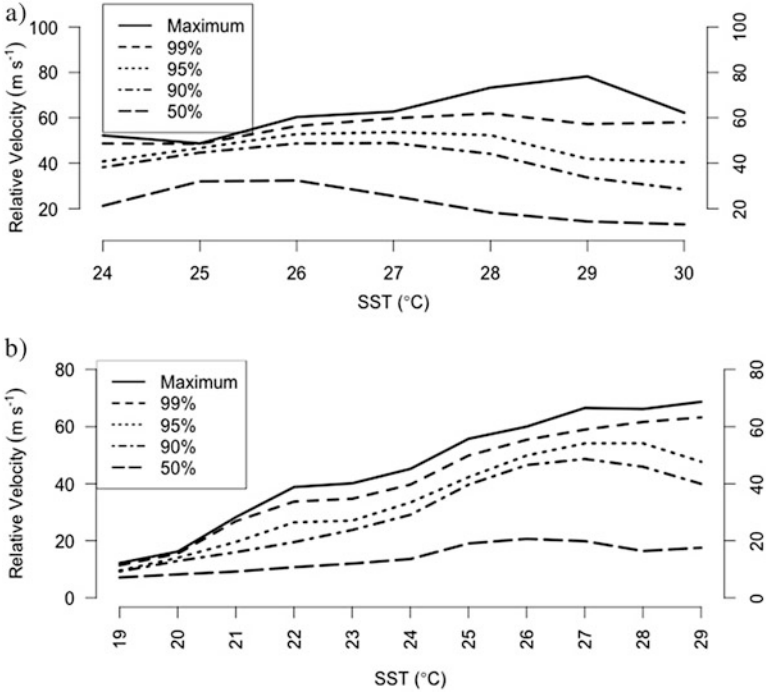
Fig. 3.19 (**a**) Same as Fig. 3.17, but only for EDR storm observations and (**b**) same as Fig. 3.17, but only for WDR storm observations

maximum intensity as a function of SST category when local storms are regionally divided. Based on the above findings, the MPI in the EDR (ENPMPI$_e$) and the WDR (ENPMPI$_w$) may require different empirical models than that performed for the entire basin. Due to a limited record of maximum TC intensity associated with each SST bin (Table 3.5), only data from 24 to 30 °C bins are used for ENPMPI$_e$. By examining the LOWESS curve (Fig. 3.20), it appears a linear function is still the most suitable function in describing the data distribution (up to 29 °C) for ENPMPI$_e$, with an equation of

$$ENPMPI_e = A_e \, (SST_e) + B_e, \tag{3.3}$$

where ENPMPI$_e$ (m s^{-1}) has a constant of $B_e = -35.756$ m s^{-1} and $A_e = 3.64$ m s^{-1} °C^{-1}. However, compared with ENPMPI, ENPMPI$_e$'s residual standard error has grown to 7.637 m s^{-1}. An ANOVA was attempted to compare the difference in residual error between a linear and a curve (polynomial) fit. Though a curve fit leads to a smaller error (3.73 m s^{-1}), it is not statistically different from the error associated with a linear function fit ($p > 0.05$).

For WDR observations, while the distribution of maximum TC intensity is observed to shift towards higher SST bins, the LOWESS curve indicates the growth
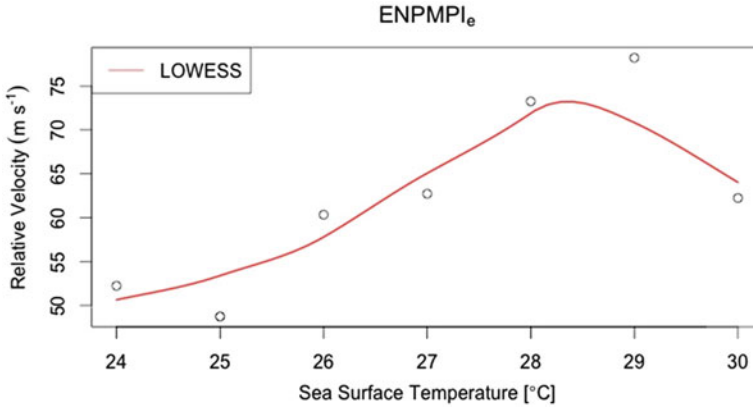
Fig. 3.20 Scatterplot for maximum storm intensity attained by each SST bin of all EDR observations. A locally weighted scatterplot smoothing (LOWESS) is applied

rate of maximum TC intensity starts to slow at the 26 °C SST bin. Interestingly, this is also generally observed as the minimum SST requirement for TC genesis and development (Palmén 1948; Dare and McBride 2011b). This flattening of growing maximum TC intensity appears to initiate at even cooler SST bins for the lower percentile curves (Fig. 3.19b). As such, even with a higher SST, other environmental influences may be more important in determining the ultimate maximum TC intensity. When linear and quadratic (curve) functions are compared for data fitting, both functions had parameter estimates that are found to be highly statistically significant. Overall, the ANOVA results indicate that the reduced predicted error of a quadratic fit is significantly lower than that of a linear function ($p < 0.01$). Thus, a linear function is deemed inadequate to represent $ENPMPI_w$. Instead, an exponential decay (increase form) function is found to be more suitable with the following equation:

$$ENPMPI_w = C_w + B_w e^{-A_w(SST-T_o)}, \tag{3.4}$$

where T_o (°C) is specified as the reference temperature and A_w, B_w and C_w are constants of the parameter estimates. With $T_o = 29$ as the highest SST bin, using a non-linear least-squares fit, $A_w = 100.40171$, $B_w = -29.90966$ and $C_w = 0.11039$. Figure 3.21 shows the data and the fitted function for $ENPMPI_w$, with a residual standard error of 2.764 m s^{-1}. Comparatively, a linear regression fit generated an error of 4.192 m s^{-1}. The choice of the exponential decay function in the form of (3.4) is indicative of the flattening of the fitted curve, starting at the 26 °C SST bin. Though it was not taken into consideration for the function fit, the reduced slope is also evident for North Atlantic storms at SST bins above 28 °C (DeMaria and Kaplan 1994). In our case, due to data limitations, there remains some uncertainty for the reduced growth to continue beyond the 29 °C bin, the reference SST bin below which $ENPMPI_w$ applies.
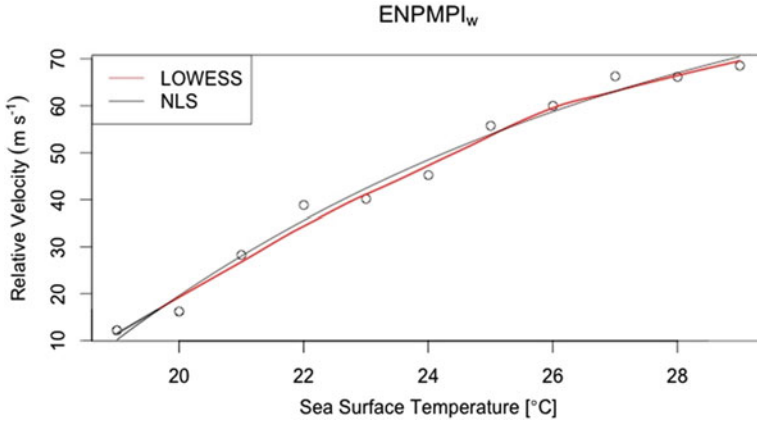
Fig. 3.21 Non-linear least-squares (NLS) fitting of maximum storm intensities bounded by SST bins at WDR, with the LOWESS curve added

7   Outflow Temperature

In addition to SST, TC maximum potential intensity is also limited by the outflow temperature near the tropopause for various TC basins (Wing et al. 2015). A cooler outflow temperature provides a more efficient mechanism at raising MPI through the effective removal of energy at the storm top. The calculation of the outflow temperature relies on surface conditions of SST and sea-level pressure, as well as temperature, pressure and relative humidity at various tropospheric levels (Bister and Emanuel 1998). Data used to construct an environmental sounding in the spatial-temporal overlap of the six-hourly ENP storm tracks are obtained from the NCEP North American Regional Analysis (Mesinger et al. 2006).

Through studies using reanalyzed atmospheric data (Wing et al. 2007, 2015; Emanuel et al. 2013) and idealized experiments in modelling the storm's environment (Ramsay 2013; Wang et al. 2014), it has been shown that maximum TC winds (minimum sea-level pressure) have noticeably increased (reduced) with decreasing outflow temperature. In contrast to the upper-tropospheric condition, the slowly increasing North Atlantic SST demonstrates the cooling of the outflow temperature is relatively more important in contributing to the recent increase in the potential intensity of North Atlantic storms (Emanuel et al. 2013). However, the consistency of the rising North Atlantic potential intensity derived from the NCEP-reanalyzed data has been challenged when data from other reanalysis products were compared (Vecchi et al. 2013).

To compare the regional difference of outflow temperature in the ENP basin, Fig. 3.22 shows the recent trend of the outflow temperature at two central locations that were arbitrarily selected to represent the EDR, at 10°N 105°W, and WDR, at 10°N 125°W. Overall, the WDR representation demonstrates a significant cooling of nearly 6 °C between 1982 and 2015, while the EDR representation has only

Fig. 3.22 The outflow temperatures (1982–2015) required to achieve theoretical maximum potential intensity at 10°N 105°W and 10°N 125°W are plotted to represent locations in EDR and WDR respectively
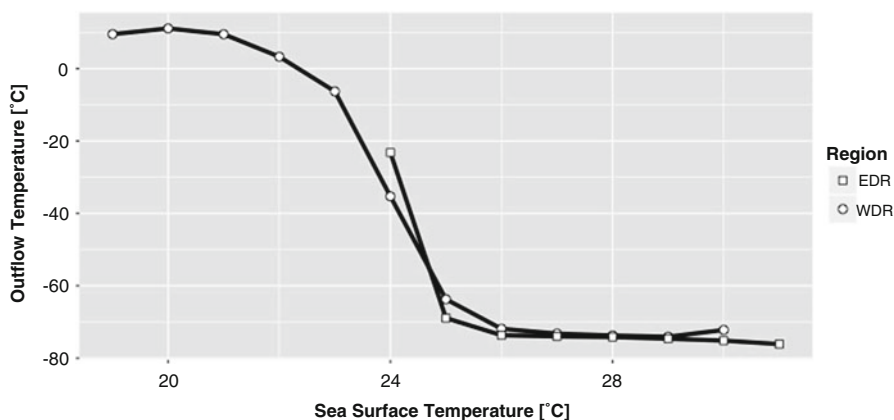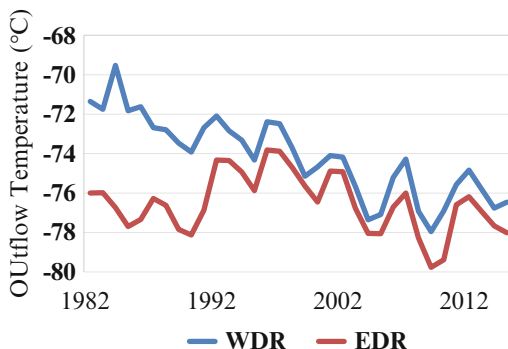

Fig. 3.23 The relationship of outflow temperatures vs. SSTs that is required to reach maximum potential intensity for EDR and WDR storm observations (1982–2013)

experienced one-fourth of the WDR's cooling rate during the same period. A greater rate of cooling in the outflow temperature reveals the overall WDR has become less stabilized, supporting a more favourable upper-atmospheric environment for storm development, as reflected in the growing number of ENP major hurricanes towards the end of the twentieth century (Collins and Mason 2000). This cooling trend lends support to the earlier analysis in which the recent increase in the maximum storm intensity is attained at each SST category in the WDR. Although Fig. 3.22 does not reflect the outflow temperatures required to establish MPI along existing storm tracks, such regional difference in the upper-tropospheric temperature offers support for the relative difference of storm intensities between EDR and WDR.

To test if the outflow temperature that is required to achieve theoretical MPI varies within the ENP basin, Fig. 3.23 plots the outflow temperatures of EDR and WDR storm observations against SSTs. During the 1982–2013 period, the averaged outflow temperature as a function of SST category reflects a slightly

cooler outflow temperature at the 25–30 °C SST interval in the EDR, where stronger maximum surface wind speed and lower minimum sea-level pressure were empirically determined. When data of both regions are combined, the shape of data distribution is similar to WDR and resembles a reversed (negative) sigmoid curve, which does not entirely resemble the SST-outflow temperature relationship from Whitney and Hobgood (1997). In particular, our analysis shows the out-flow temperatures of WDR storms associated with SSTs below the 24 °C bin exhibit a warmer atmosphere near the cloud top. This is reflected by a rapid decrease of the upper-tropospheric temperature within a SST range between 23.5 and 25.5 °C. The slow-cooling outflow regions, corresponding to SSTs higher than 25.5 °C, is reflected by a slower increase in the maximum WDR storm winds (Fig. 3.21). As such, this empirically calculated MPI at the highest SST condition is rarely obtained through real-time storm observations and could also vary due to storm track variability (Wing et al. 2007, 2015; Kossin and Camargo 2009).

8 Conclusions

For TC development basins worldwide, SSTs have been recognized, directly (Evans 1993) and indirectly through ENSO influences (Chu 2004), as the major thermodynamic limit of maximum TC intensity. While local SST increase tends in general to elevate storm intensity, remote SST changes (Vecchi and Soden 2007) and upper-tropospheric temperatures (Bister and Emanuel 1998) could enforce significant impacts on the upper limit of TC intensity. As the long-term conditions of the ocean surface shift to a warmer condition, TC intensities are expected to strengthen with SST increase. Although the spatial-temporal resolution of SST data has remained a challenge in pinpointing the SST condition underlying storm tracks, near-time (daily) SST data with a spatial resolution of 0.25° by 0.25° are employed to document its extent of impact on ENP storm winds. Due to the spatial sensitivity of ENP storm intensity to environmental conditions, the limiting effect of SST on ENP storm strength is demonstrated to vary within this region. Because the inhibiting effect of the rate of SST decrease is stronger (weaker) during EDR (WDR) storm passage, the SST impact on TC intensity is greater for WDR storm observations and their maximum lifetime intensities.

Two ways of exploring the SST-TC intensity relationship are presented in the study: (1) correlating SST values with TC intensity and (2) stratifying TC observations into SST bins of 1 °C interval and then relating TC intensities of all TC data points with SST category. Although the direct SST measurement is not the only factor contributing to TC intensity, this association for ENP storms is stronger than that of North Atlantic storms. Using the linear least-squares regression, the results of the study indicate a statistically significant relationship exists between SST and TC intensity. Alternatively, though SST anomalies calculated by subtracting local SST from the ENP Main Development Region (MDR) SST average have been recently

demonstrated to have a greater association with local storm count and intensity (Zhang and Wang 2015), the effect of relative SST as an anomaly from the zonal-mean SST and its impact on the regional sensitivity of ENP storm intensities are still unknown. Further investigation of the maximum lifetime intensity of major hurricanes shows the SST influence on TC intensity is greatest for the most intense storms. Stratification of TC winds according to near-time SST bins supports the previous finding of the SST-dependent MPI in the ENP basin, indicating a stronger relationship when the most recent TC climatology is compared to the past.

Under a regional difference in SST conditions, ENP storms are longitudinally divided to understand regional sensitivity of storm intensity to an SST limit. Compared to the EDR, intensities for WDR storm observations are more responsive to SST fluctuations. When the maximum winds of WDR storms are considered and categorized into different levels of TC intensity, major hurricanes display a stronger association with contemporaneous SST values. In contrast to the North Atlantic region where an absence of such a relationship was found (Michaels et al. 2006), subdividing MDR has facilitated a regional variation in which the maximum TC intensity is correlated with SST. An examination of minimum SST requirements to achieve certain TC strengths also reveals regionally distinct SST ranges to achieve peak intensities for hurricanes and major hurricanes. Compared to the SST limit (28.25 °C) for attaining major hurricanes in the North Atlantic basin, lower SST values are observed where most of the EDR (27 °C) and WDR (25 °C) major hurricanes are established in the ENP.

In contrast to Whitney and Hobgood (1997), an updated ENP storm climatology reveals that the relationship between the outflow temperature and corresponding SST required to attain theoretical MPI is non-linear even when storm groups are longitudinally divided. While the association between maximum storm intensity with SST has increased with a changing climate, when the ENP MDR is subdivided, such linkage is stronger for WDR storm observations until a certain SST limit is approached. Part of this observed relationship may be attributed to a less potent SST reduction inflicted by WDR storm passages. However, such a contrast in the regional TC intensity can also be steered by the outflow temperature near cloud tops. Past the 25 °C SST bin, where the maximum storm intensities of most WDR major hurricanes would have already been sustained, the decay in the growth rate of MPI is marked by a slower reduction of the outflow temperature in the upper troposphere.

Despite a downward trend experienced in the transport of EDR-originated WDR storms, SST warming supports the strengthening of the strongest storms. However, WDR storms indicate such a response becomes non-linear with a slower rate of increase as warmer SSTs are approached. In addition, the association of TC intensity to SST is further challenged by observations of relatively weak intensity over warm SSTs before progressing and intensifying over cooler waters. As such, future studies involving the thermodynamic limit of TC intensity may need to incorporate the ocean heat content by taking into account of not only SST but also energy generated across the entire thermocline depth (Balaguru et al. 2013; Jin et al. 2014). The incorporation of the total ocean heat content may reveal a latitudinal, as opposed to longitudinal, contrast in the relationship of SST-TC

intensity (Balaguru et al. 2013). Although other atmospheric factors could also have an important role in modifying TC intensity, the application of near-time SST greatly contributes to the understanding that, in addition to the regional difference of SST requirement for genesis and intensification of major hurricanes, the eventual intensity of major hurricanes in the WDR are greatly limited by SST conditions encountered prior to the peak of its lifetime intensity.

With the realization of higher maximum lifetime intensity and MPI under the future scenario of continuous SST warming, future increase of ocean temperatures may raise the intensity of damaging storm winds. Since stronger storms tend to be sustained over longer distances, SST warming may also lengthen TC influence for a greater spatial extent. Upon landfall, storm tracks may extend further inland, posing a direct threat to coastal safety. From a forecasting point of view, the possibility of an extended TC influence upon landfalling TCs may result in the broadening of uncertainties associated with near-time projection of storm path. Consider as the strongest TC to exist in the western hemisphere since the satellite era, Hurricane Patricia (2015), as well as other potent storms, had reinvigorated efforts at further investigating the ENP storm outlook under a continuously evolving climate.

References

Balaguru K, Leung LR, Yoon J-H (2013) Oceanic control of northeast Pacific hurricane activity at interannual timescales. Environ Res Lett 8:4009. doi:10.1088/1748-9326/8/4/044009

Bender MA, Ginis I (2000) Real-case simulations of hurricane–ocean interaction using a high-resolution coupled model: effects on hurricane intensity. Mon Weather Rev 128:917–946

Bister M, Emanuel KA (1998) Dissipative heating and hurricane intensity. Meteorol Atmos Phys 65:233–240

Boucharel J, Jin F-F, Lin II, Huang H-C, England MH (2016) Different controls of tropical cyclone activity in the Eastern Pacific for two types of El Niño. Geophys Res Lett. doi:10.1002/2016GL067728

Caron L-P, Boudreault M, Camargo SJ (2015) On the variability and predictability of eastern north Pacific tropical cyclone activity. J Climate 28:9678–9696

Chu P-S (2004) ENSO and tropical cyclone activity. In: Murnane RJ, Liu KB (eds) Hurricanes and typhoons: past, present, and potential. Columbia University Press, New York, pp 297–332

Cione JJ, Uhlhorn EW (2003) Sea surface temperature variability in hurricanes: implications with respect to intensity change. Mon Weather Rev 131:1783–1796

Collins J (2010) Contrasting high North-East Pacific tropical cyclone activity with low North Atlantic activity. Southeast Geogr 50:83–98

Collins JM, Mason IM (2000) Local environmental conditions related to seasonal tropical cyclone activity in the Northeast Pacific basin. Geophys Res Lett 27:3881–3884

Collins JM, Roache DR (2011) The 2009 hurricane season in the eastern North Pacific basin: an analysis of environmental conditions. Mon Weather Rev 139(6):1673–1681

Dare RA, Mcbride JL (2011a) Sea surface temperature response to tropical cyclones. Mon Weather Rev 139(12):3798–3808

Dare RA, Mcbride JL (2011b) The threshold sea surface temperature condition for tropical cyclogenesis. J Climate 24(17):4570–4576

Davis MAS, Brown GM, Leftwich P (1984) A tropical cyclone data tape for the eastern and Central North pacific basins, 1949–1983: contents, limitations, and uses. NOAA Technical Memorandum NWS NHC 25, http://www.nhc.noaa.gov/pdf/NWS-NHC-1984-25.pdf

DeMaria M, Kaplan J (1994) Sea surface temperature and the maximum intensity of Atlantic tropical cyclones. J Climate 7:1325–1334

Diamond HJ, Lorrey AM, Renwick JA (2013) A southwest Pacific tropical cyclone climatology and linkages to the El Niño–Southern Oscillation. J Climate 26:3–25

Emanuel KA (1987) The dependence of hurricane intensity on climate. Nature 326(6112):483–485

Emanuel KA (2005) Increasing destructiveness of tropical cyclones over the past 30 years. Nature 436:686–688

Emanuel K, Solomon S, Folini D, Davis S, Cagnazzo C (2013) Influence of tropical tropopause layer cooling on Atlantic hurricane activity. J Climate 26:2288–2301

Evans JE (1993) Sensitivity of tropical cyclone intensity to sea surface temperature. J Climate 6:1133–1140

Goldenberg SB, Landsea CW, Mestas-Nuñez AM, Gray WM (2001) The recent increase in Atlantic hurricane activity: causes and implications. Science 293:474–479

Gray WM (1968) A global view of the origin of tropical disturbances and storms. Mon Weather Rev 96:669–700

Gray WM (1984) Atlantic seasonal hurricane frequency: part I. El Nino and 30 mb quasi-biennial oscillation influences. Mon Weather Rev 112:1649–1668

Hart RE, Maue RN, Watson MC (2007) Estimating local memory of tropical cyclones through MPI anomaly evolution. Mon Weather Rev 135(12):3990–4005

Henderson-Sellers A et al (1998) Tropical cyclones and global climate change: a post-IPCC assessment. Bull Am Meteorol Soc 79:19–38

Jien J, Gough WA, Butler K (2015) The influence of El Niño-Southern Oscillation on tropical cyclone activity in the eastern North Pacific basin. J Climate 28(16):2459–2474

Jin F-F, Boucharel J, Lin II (2014) Eastern Pacific tropical cyclones intensified by El Niño delivery of subsurface ocean heat. Nature 516:82–85

Kaplan J, DeMaria M, Knaff JA (2010) A revised tropical cyclone rapid intensification index for the Atlantic and eastern north Pacific basins. Weather Forecast 25(1):220–241

Kossin JP, Camargo SJ (2009) Hurricane track variability and secular potential intensity trends. Clim Change 9:329–337

Kotal SD, Kundu PK, Bhowmik SKR (2009) An analysis of sea surface temperature and maximum potential intensity of tropical cyclones over the Bay of Bengal between 1981 and 2000. Meteorol Appl 16(2):169–177

Landsea CW, Franklin JL (2013) Atlantic hurricane database uncertainty and presentation of a new database format. Mon Weather Rev 141(10):3576–3592

Landsea CW, Bell GD, Gray WM, Goldenberg SB (1998) The extremely active 1995 atlantic hurricane season: environmental conditions and verification of seasonal forecasts. Mon Weather Rev 126(5):1174–1193

Martinez-Sanchez JN, Cavazos T (2014) Eastern tropical Pacific hurricane variability and landfalls on Mexican coasts. Climate Res 58(3):221–234

Maue RN (2009) Northern hemisphere tropical cyclone activity. Geophys Res Lett 36(5):L05805. doi:10.1029/2008GL035946

Mei W, Pasquero C (2013) Spatial and temporal characterization of sea surface temperature response to tropical cyclones. J Climate 26(11):3745–3765

Mei W, Pasquero C, Primeau F (2012) The effect of translation speed upon the intensity of tropical cyclones over the tropical ocean. Geophys Res Lett 39:L07801. doi:10.1029/2011GL050765

Merrill RT (1988) Environmental influences on hurricane intensification. J Atmos Sci 45:1678–1687

Mesinger F et al (2006) North American regional reanalysis. Bull Am Meteorol Soc 87(3):343–360

Michaels PJ, Knappenberger PC, Davis RE (2006) Sea-surface temperatures and tropical cyclones in the Atlantic basin. Geophys Res Lett 33(9):L09708. doi:10.1029/2006GL025757

Miller BI (1958) On the maximum intensity of hurricanes. J Meteor 15:184–195

Molinari J, Knight D, Dickenson M, Vollaro D, Skubis S (1997) Potential vorticity, easterly waves and eastern Pacific intensification. Mon Weather Rev 125:2699–2708

Palmén E (1948) On the formation and structure of tropical hurricanes. Geophysica 3:26–38

Patricola C, Saravanan R, Chang P (2014) The impact of the El Niño–Southern Oscillation and Atlantic meridional mode on seasonal Atlantic tropical cyclone activity. J Climate 27:5311–5328

Raga GB, Bracamontes-Ceballos B, Farfán LM, Romero-Centeno R (2013) Landfalling tropical cyclones on the Pacific coast of Mexico: 1850–2010. Atmosfera 26(2):209–220

Ralph TU, Gough WA (2009) The influence of sea-surface temperatures on eastern North Pacific tropical cyclone activity. Theor Appl Climatol 95:257–264

Ramsay HA (2013) The effects of imposed stratospheric cooling on the maximum intensity of tropical cyclones in axisymmetric radiative–convective equilibrium. J Climate 26:9977–9985

Saunders MA, Lea AS (2008) Large contribution of sea surface warming to recent increase in Atlantic hurricane activity. Nature 451(7178):557–560

Thorncroft C, Hodges K (2001) African easterly wave variability and its relationship to Atlantic tropical cyclone activity. J Climate 14:1166–1179

Vecchi GA, Soden BJ (2007) Effect of remote sea surface temperature change on tropical cyclone potential intensity. Nature 450(7172):1066–1070

Vecchi GA, Fueglistaler S, Held IM, Knutson TR, Zhao M (2013) Impacts of atmospheric temperature changes on tropical cyclone activity. J Climate 26:3877–3891

Wang S, Camargo SJ, Sobel AH, Polvani LM (2014) Impact of the tropopause temperature on the intensity of tropical cyclones – an idealized study using a mesoscale model. J Atmos Sci 71:4333–4348

Webster PJ, Holland GJ, Curry JA, Chang H-R (2005) Changes in tropical cyclone number, duration, and intensity in a warming environment. Science 309:1844–1846

Whitney LD, Hobgood JS (1997) The relationship between sea surface temperatures and maximum intensities of tropical cyclones in the eastern north Pacific Ocean. J Climate 10(11):2921–2930

Wing AA, Sobel AH, Camargo SJ (2007) The relationship between the potential and actual intensities of tropical cyclones on interannual time scales. Geophys Res Lett 34:L08810. doi:10.1029/2006GL028581

Wing AA, Emanuel K, Solomon S (2015) On the factors affecting trends and variability in tropical cyclone potential intensity. Geophys Res Lett 42:8669–8677. doi:10.1002/2015GL066145

Wood KM, Ritchie EA (2013) An updated climatology of tropical cyclone impacts on the southwestern United States. Mon Weather Rev 141:4322–4336

Wu L, Tao L, Ding Q (2010) Influence of sea surface warming on environmental factors affecting long-term changes of Atlantic tropical cyclone formation. J Climate 23(22):5978–5989

Xie S-P, Deser C, Vecchi GA, Ma J, Teng H, Wittenberg AT (2010) Global warming pattern formation: sea surface temperature and rainfall. J Climate 23(4):966–986

Zeng Z, Wang Y, Wu C-C (2007) Environmental dynamical control of tropical cyclone intensity – an observational study. Mon Weather Rev 135(1):38–59

Zhang G, Wang Z (2015) Interannual variability of tropical cyclone activity and regional Hadley circulation over the northeastern Pacific. Geophys Res Lett 42:2473–2481